JPET Fast Forward. Published on March 6, 2008 as DOI: 10.1124/jpet.108.136895

Synthesis and characterization of [^{125}I]α-conotoxin ArIB[V11L;V16A], a selective α7 nAChR antagonist.

Paul Whiteaker, Michael J. Marks, Sean Christensen, Cheryl Dowell, Allan C. Collins and *J. Michael McIntosh.

Division of Neurobiology, Barrow Neurological Institute, Phoenix, AZ, 85013 (P.W.). Institute for Behavioral Genetics, University of Colorado, Boulder, CO 80309 (M.J.M., A.C.C.). Departments of Biology (S.C., S.D., J.M.M.) and Psychiatry, University of Utah, Salt Lake City, UT 84112 (J.M.M.).

Running title: Novel nicotinic α7 receptor ligand

*Corresponding author: J Michael McIntosh, University of Utah 257 S. 1400 E. Salt Lake City, Utah 84112. Phone: (801) 585-3622. Fax: (801)-585-5010. Email: mcintosh.mike@gmail.com

Text Pages: 37

Tables: 0

Figures: 6

References: 25

Words in Abstract: 245

Words in Introduction: 565

Words in Discussion: 967

Abbreviations:

[I_1], monoiodo; [I_2], diiodo; α-Ctx, α-conotoxin; α-Bgt, α-bungarotoxin; MLA, methyllycaconitine.

JPET Fast Forward. Published on March 6, 2008 as DOI: 10.1124/jpet.108.136895
This article has not been copyedited and formatted. The final version may differ from this version.

ABSTRACT:

α7 nAChRs are widely expressed both in the central nervous system (CNS) and periphery. In the CNS, [^{125}I]α-bungarotoxin is commonly used to identify α7 nAChRs specifically. However, α-bungarotoxin also interacts potently with α1* and α9α10 nAChRs, two receptor subtypes in peripheral tissues that are co-localized with the α7 subtype. [^{3}H]Methyllycaconitine is also frequently used as an α7-selective antagonist, but has significant affinity for α6* and α9α10 nAChRs subtypes. Here, we have developed a highly α7 selective α-conotoxin radioligand by iodination of a naturally occurring histidine. Both mono- and diiodo derivatives were generated and purified (specific activities were 2200 and 4400 Ci mmol^{-1}, respectively). The properties of the mono- and diiodo derivatives were very similar to each other, but the diiodo was less stable. For monoidodo peptide, saturation binding to mouse hippocampal membranes demonstrated a K_d of 1.15 ± 0.13 nM, similar to that of [^{125}I]α-bungarotoxin in the same preparations (0.52 ± 0.16 nM). Association and dissociation kinetics were relatively rapid (k_{obs} for association at 1 nM was 0.027 ± 0.007 min^{-1}; k_{off} = 0.020 ± 0.001 min^{-1}). Selectivity was confirmed with autoradiography using α7-null mutant tissue: specific binding was abolished in all regions of α7$^{-/-}$ brains, while wildtype mice expressed high levels of labeling and low non-specific binding. [^{125}I]α-Conotoxin ArIB[V11L;V16A] should prove useful where α7 nAChRs are co-expressed with other subtypes that are also labeled by existing ligands. Further, true equilibrium binding experiments could be performed on α7 nAChRs, something that is impossible with [^{125}I]α-bungartoxin.

JPET Fast Forward. Published on March 6, 2008 as DOI: 10.1124/jpet.108.136895
This article has not been copyedited and formatted. The final version may differ from this version.

INTRODUCTION:

α-Bungarotoxin (α-Bgt), a peptide neurotoxin from the venom of the Taiwanese banded krait *Bungarus multicinctus*, has a long and successful history in nicotinic receptor studies. Originally, α-Bgt was used to identify and characterize the muscle-type nAChR, at which it is a potent (nanomolar K_i) competitive antagonist (Changeux et al., 1970). Later, [^{125}I]α-Bgt was used to identify the first mammalian neuronal nAChRs (Salvaterra and Mahler, 1976), although this classification was initially controversial (Clarke, 1992). It is now established that mammalian central nervous system [^{125}I]α-Bgt binding sites correspond to α7* nAChRs (where * denotes the possible presence of additional subunits, although α7 nAChRs are most likely homomeric; Chen and Patrick, 1997).

Despite this successful track-record, it has become apparent that α-Bgt has some disadvantages. For instance, α-Bgt also binds with similar affinity to α8* (Gotti et al., 1994) and α9α10 nAChRs (Elgoyhen et al., 2001) as it does to the α1 muscle-type and α7 neuronal nAChRs already mentioned. Neuronal nAChR expression and effects outside of the brain / CNS are areas of increasing interest, and α7 nAChR gene and / or protein expression has been shown to overlap with that of the α-Bgt-sensitive α9α10 subtype in cochlea (Morley et al., 1998), dorsal root ganglion (Haberberger et al., 2004), keratinocytes (Nguyen et al., 2000), and lymphocytes (Peng et al., 2004). In addition, injured muscle co-expresses muscle-type (α1*) and α7 nAChR subtypes (Martyn and Richtsfeld, 2006) both of which bind α-Bgt with high affinity. Further, the exceptionally slow binding kinetics of [^{125}I]α-Bgt to α7 nAChRs (Salvaterra and Mahler, 1976) make true equilibrium binding studies impractical.

Accordingly, alternatives to α-Bgt in identifying α7 nAChRs have been sought. The norditerpenoid alkaloid methyllycaconitine (MLA) isolated from *Delphinium* sp. is a

JPET Fast Forward. Published on March 6, 2008 as DOI: 10.1124/jpet.108.136895
This article has not been copyedited and formatted. The final version may differ from this version.

competitive antagonist for α7 nAChRs, at which it has approximately nM affinity and more useful kinetic properties than α-Bgt (Davies et al., 1999). Unfortunately, MLA also interacts with α6* nAChRs with relatively high affinity (Salminen et al., 2005). In the central nervous system, MLA-sensitive α6β2* nAChRs are concentrated in the dopaminergic projections of the substantia nigra and ventral tegmental area, and the optic tract (Gotti et al., 2005). These regions also contain α7 nAChRs (Clarke et al., 1985); (Pauly et al., 1989); (Quik et al., 2003), complicating efforts to identify α7 nAChRs specifically using MLA. α9α10 nAChRs are difficult to express heteromerically, but chimeric subunits (containing the N-terminal ligand binding domain of each subunit, fused in each case to the C-terminal of a 5-HT_{3A} subunit) express well and also bind [^{3}H]MLA with nanomolar affinity (Baker et al., 2004), suggesting that identification of peripheral α7 nAChRs with MLA may also suffer problems of specificity.

In a previous study (Whiteaker et al., 2007), we identified an α-conotoxin (α-CtxArIB) with some selectivity towards α7 nAChRs. Using a guided amino-acid substitution strategy, we eventually produced a pair of modified peptides (α-CtxArIB[V11L;V16A]; α-CtxArIB[V11L;V16D]) with similar-to-unmodified affinity for α7 nAChRs, but with much improved α7 selectivity. Importantly, both peptides also exhibited relatively rapid association and dissociation kinetics. In the current study, we describe the synthesis and characterization of a radioligand based on α-CtxArIB ([^{125}I]α-CtxArIB[V11L;V16A]). This peptide exhibits saturable binding, possesses similar affinity for α7 nAChRs as does [^{125}I]α-Bgt, selectively labels α7 nAChRs, and has relatively rapid association and dissociation kinetics. As such, it is likely to facilitate specific identification of α7 nAChRs in previously hard-to-study contexts, and enable the performance of true equilibrium binding experiments at α7 nAChRs.

JPET Fast Forward. Published on March 6, 2008 as DOI: 10.1124/jpet.108.136895
This article has not been copyedited and formatted. The final version may differ from this version.

METHODS:

Preparation of membranes, mouse brain sections.

Mice were bred at the Institute for Behavioral Genetics, and housed five per cage. Male mice (C57BL/6J, and mice engineered to lack α7 nAChR subunit gene expression; Franceschini et al., 2002) were used when 60 –120 days old. The vivarium was maintained on a 12 h light / dark cycle and mice were given free access to food and water. All procedures used in this study were approved by the Animal Care and Utilization Committee of the University of Colorado.

To prepare brain membranes, each mouse was sacrificed by cervical dislocation, the brain removed, and placed on an ice-cold platform. Tissue was collected from the hippocampus, olfactory tubercle, striatum, superior colliculus, thalamus and midbrain. Individual hippocampal or thalamic samples were homogenized in ice-cold hypotonic buffer (mM: NaCl, 14.4; KCl, 0.2; $CaCl_2$, 0.2; $MgSO_4$, 0.1; HEPES 2; pH = 7.5) using a glass-Teflon tissue grinder (Marks et al., 1998). Particulate fractions were collected by centrifugation at 25,000 x *g* (15 min, 4 ºC; Eppendorf 5417 C centrifuge). The pellets were resuspended in fresh homogenization buffer, incubated on ice for 10 min, then harvested by centrifugation as before. Each pellet was washed twice more by resuspension / centrifugation before storage (in pellet form under homogenization buffer) at –70 ºC until used. Pooled olfactory tubercle, striatal and superior colliculus tissue from pairs of mice was homogenized and then stored in the same way. Midbrain samples were pooled from 24 mice, then homogenized as described for hippocampi, before being divided into 24 individual aliquots and stored at –70 ºC until needed.

Frozen *Torpedo californica* electroplax tissue was obtained from Aquatic Research Consultants (San Pedro, CA). Tissue was thawed on ice, then homogenized (3 x 5 s at full speed) using a Polytron homogenizer (Brinkmann Instruments, Westbury,

NY) in ice-cold isotonic binding buffer (mM: NaCl, 144; KCl, 2; $CaCl_2$, 2; $MgSO_4$, 1; HEPES 20; pH = 7.5) supplemented with bovine serum albumin (0.1% (w/v)) and protease inhibitors (5 mM EDTA, 5 mM EGTA, 1 mM phenylmethylsulfonylfluoride and 10 µg / ml each of aprotinin, leupeptin trifluoroacetate, and pepstatin A; protease inhibitor buffer) to minimize proteolysis. Membranes were collected by centrifugation (25,000 x *g*, 30 min, 4 ºC), and the resulting pellets were rehomogenized as before. The resulting membranes were washed twice more by resuspension in protease inhibitor buffer and centrifugation before storage (in pellet form under homogenization buffer) at – 70 ºC until used.

Membranes were also prepared from *Xenopus* oocytes injected ~ 12.5 ng of each cRNA encoding rat α9 and α10 nAChR subunits (clones generously provided by A.B. Elgoyhen, Universidad de Buenos Aires). After incubation at 17 ºC for 4-5 days, transfected oocytes were frozen using liquid nitrogen (typically in batches of 40) and stored at -70 ºC until required. The approach used was a slight modification of that described by Parker et al (1998). Oocytes were thawed, suspended in 2 ml distilled water and homogenized (16 s at full speed) using a Polytron homogenizer (Brinkmann Instruments, Westbury, NY). The resulting homogenate was then centrifuged gently (2000 x *g*, 2 min) to separate it into three layers (lipids, top; membrane fragments, middle; large fragments and pigment granules, bottom). Membrane fragments were collected using a Pasteur pipette and used for binding assays.

For mouse brain sections, mice of $\alpha7^{+/+}$ and $\alpha7^{-/-}$ genotype were killed by cervical dislocation, the brains were removed from the skull and rapidly frozen by immersion in isopentane (-35°C, 10s). The frozen brains were wrapped in aluminum foil, packed in ice, and stored at -70°C until sectioning. Coronal tissue sections (14 µm thick) were obtained using a Leica (Nussloch, Germany) CM 1850 cryostat / microtome, and thaw

JPET Fast Forward. Published on March 6, 2008 as DOI: 10.1124/jpet.108.136895
This article has not been copyedited and formatted. The final version may differ from this version.

mounted onto SuperFrost glass slides (Fisher Scientific; Pittsburgh, PA). Sections were stored, desiccated, at –70 °C until used.

Choice of α-CtxArIB[V11L;V16A], His-iodination.

In our previous study, we identified an α7 nAChR subtype selective peptide, α-CtxArIB. This peptide, although moderately selective, also showed some affinity for α6/α3β2β3 nAChRs (α6/α3β2β3:α7 affinity ratio = 3.56). Accordingly, we generated a series of increasingly more α7-selective derivatives. Of these derivatives, the two most selective were α-CtxArIB[V11L;V16A] (functional IC_{50} value at α7 = 0.356 nM; α6/α3β2β3:α7 affinity ratio = 337) and α-CtxArIB[V11L;V16D] (functional IC_{50} value at α7 = 1.09 nM; α6/α3β2β3:α7 affinity ratio = 760 (Whiteaker et al., 2007)). We chose α-CtxArIB[V11L;V16A] as a starting point for the generation of a radiolabeled, α7-selective α-CtxArIB derivative since it is highly α7-selective but has higher affinity than α-CtxArIB[V11L;V16D].

α-CtxArIB and each of its derivatives contain a single histidine residue (at position 15; (Whiteaker, et al., 2007)), which represents a potential iodination site. Before attempting radioiodination at this native residue, we first cold-iodinated α-CtxArIB[V11L;V16A] to see if this affected the affinity of α-CtxArIB[V11L;V16A] for α7 nAChRs.

Synthesis of α-CtxArIB[V11L;V16A] was performed as previously described (Whiteaker et al., 2007). To iodinate the peptide, 5 nmol of α-CtxArIB[V11L;V16A] was dissolved in 10 µl of 0.25 mM Tris, pH 8.2. To this was added 15 µl of 0.4 mM NaI or 5 mCi of $Na^{125}I$ (volume ~15 µl, specific activity ~2200 Ci / mmol; PerkinElmer Life and Analytical Sciences, Inc, Wellesley, MA). The iodination reaction was initiated by the addition of 12.5 µl of freshly prepared 4 mM Chloramine-T (*p*-toluene

sulfonochloramide). The water soluble Chloramine-T provides a more easily controlled iodination reaction than the alternative insoluble reagent iodogen. The reaction proceeded at room temperature for 40 min and then was quenched by the addition of 65 µl of freshly prepared 0.5 M ascorbic acid. The pH of the reaction mixture was further lowered by the addition of 0.8 ml of 0.1% trifluoroacetic acid (TFA). Monoiodinated and diiodinated peptides were separated from unmodified peptide by reversed-phase HPLC using an analytical C18 column (Vydac). Buffer A was 0.1% TFA, buffer B was 0.092% TFA, 60% acetonitrile. The gradient was 10 - 50% buffer B over 40 min. Flow rate was 1 ml/ min and the absorbance was monitored at 220 nM. For purification of radioactive peptide a solution of 2.5% sodium thiosulfate and 0.2% potassium iodide in 1 N NaOH was added to the waste collection beaker to trap unreacted ^{125}I. Fractions containing mono- and diiodinated peptide were collected in siliconized tubes containing 10 µl of 20 mg / ml lysozyme to minimize absorption to the tubes. Using the above chromatographic conditions, the unmodified peptide elutes at approximately 30.8% B, the monoiodinated peptide at approximately 31.5% B, and the diiodinated peptide at approximately 33.8% B. Final yield for the cold reaction was approximately 2 nmol of monoiodo peptide and 1 nmol of diiodo peptide, and for the hot reaction, 0.5 nmol of monoiodo peptide and 0.3 nmol of diiodo peptide. Mono- and diiodination of α-CtxArIB[V11L;V16A] was verified by matrix-assisted laser desorption ionization time-of-flight mass spectrometry at the Salk Institute for Biological Studies (San Diego, CA) under the direction of Jean Rivier.

Measurement of His-iodination (non-radioactive) effects on α7 affinity.

The effects of His iodination (using non-radioactive iodide) on α-CtxArIB[V11L;V16A] affinity for α7 subtype nAChRs were determined using inhibition binding experiments. Peptide concentration ranges were: α-CtxArIB[V11L;V16A], 0.3 nM

JPET Fast Forward. Published on March 6, 2008 as DOI: 10.1124/jpet.108.136895
This article has not been copyedited and formatted. The final version may differ from this version.

– 10 μM; [I_1]α-CtxArIB[V11L;V16A] and [I_2]α-CtxArIB[V11L;V16A], 0.03 nM to 1 μM. Protocols followed were very similar to those previously described (Whiteaker, et al., 2007). Affinity for α7 nAChRs was measured by displacement of [^{125}I]α-Bgt binding to hippocampal membranes. Incubations were performed at 22 ºC for 4 h in 1.2 ml polypropylene tubes arranged in a 96-well format. Hippocampal membranes were incubated with 2 nM monoiodinated α-Bgt ([$^{125}I_1$]α-Bgt, 2000 Ci mmol^{-1}; GE Healthcare, Piscataway NJ) in a total volume of 30 μl of protease inhibitor buffer to minimize proteolysis. Displacement of [^{125}I]α-Bgt binding was assessed in duplicate. Total (no peptide added) and non-specific binding (defined using 10 μM α-cobratoxin) was also measured in duplicate. Following the initial incubation, 1 ml of isotonic binding buffer, supplemented with bovine serum albumin (0.1% (w/v)) was added to each tube and the incubation was continued for a further 5 min at 22 ºC. This dilution and further incubation step allows some of the non-specific [$^{125}I_1$]α-Bgt binding to dissociate, but has no measurable effect on specific binding, increasing the signal : noise ratio of the binding assay. Binding reactions were terminated by filtration using a 96-place manifold (Inotech Biosystems, Lansing, MI). Particulate fractions were collected onto single layers of Inotech 0.75 μm retention glass fiber filters that had been soaked in 5% nonfat skim milk dissolved in isotonic binding buffer. Samples were washed six times, and all filtration and washing steps were conducted in a 4 ºC cold room, using ice-cold buffer. Bound radioligand was quantified by gamma counting at 83 – 85% efficiency, using a Packard Cobra counter (PerkinElmer Life and Analytical Sciences, Inc, Wellesley, MA).

[^{125}I]α-CtxArIB[V11L;V16A] association and dissociation kinetics.

First, the association kinetics of specific [$^{125}I_1$]α-CtxArIB[V11L;V16A] and [$^{125}I_2$]α-CtxArIB[V11L;V16A] binding to hippocampal membranes were measured. Hippocampal tissue was chosen because it expresses high concentrations of α7 nAChRs, is relatively

JPET Fast Forward. Published on March 6, 2008 as DOI: 10.1124/jpet.108.136895
This article has not been copyedited and formatted. The final version may differ from this version.

large, and is simple to dissect. To minimize non-specific binding, and reduce the possibility of labeling putative lower-affinity receptor populations, a low (1 nM) radioligand concentration of [^{125}I]α-CtxArIB[V11L;V16A] was used. Incubations proceeded for 2 – 180 min in a total volume of 30 µl of isotonic binding buffer supplemented with protease inhibitors in 96-well polypropylene plates. At each time point, total (no added drug) and non-specific (in the presence of 10 µM α-cobratoxin) binding was measured in triplicate. Binding reactions were terminated by filtration using a 96-place manifold (Inotech Biosystems, Lansing, MI). Particulate fractions were collected onto single layers of Inotech 0.75 µm retention glass fiber filters that had been soaked in 5% nonfat skim milk dissolved in isotonic binding buffer. Alternative filter preparations were piloted (filters soaked in binding buffer alone, or soaked in 0.5% (w/v) polyethylenimine) but these produced higher non-specific binding and were not used (data not shown). Samples were washed six times, in a 4 ºC cold room, using ice-cold buffer. Bound radioligand was quantified by gamma counting at 83 – 85% efficiency, using a Packard Cobra counter (PerkinElmer Life and Analytical Sciences, Inc, Wellesley, MA).

Dissociation kinetics were measured similarly. Hippocampal membranes were first incubated with radioligand (1 nM) for 2 h (long enough for equilibrium binding to be closely approached, as revealed by the association kinetics experiments), in the same configuration as described for the association experiments. Total (no added drug) and non-specific binding (in the presence of 10 µM α-cobratoxin) triplicates were set up for each dissociation time point. Dissociation was initiated by the addition of 10 µl of 40 µM α-cobratoxin to each well, and was allowed to proceed for 2 – 180 min before sample collection, washing, and radioactivity counting as described for the association experiments.

JPET Fast Forward. Published on March 6, 2008 as DOI: 10.1124/jpet.108.136895
This article has not been copyedited and formatted. The final version may differ from this version.

[^{125}I]α-CtxArIB[V11L;V16A] saturation binding.

Saturation binding experiments were performed for [$^{125}I_1$]α-CtxArIB[V11L;V16A] and [$^{125}I_2$]α-CtxArIB[V11L;V16A], using mouse hippocampal membranes as a source of α7 nAChRs. For comparison, saturation of [$^{125}I_1$]α-Bgt binding was assessed in parallel. A slightly modified version of the [$^{125}I_1$]α-Bgt binding assay described previously was used. Incubations were performed at 22 ºC in 1.2 ml polypropylene tubes arranged in a 96-well format, but proceeded for 2 h. Membranes were incubated with a range of radioligand concentrations (approximately 0.04 – 4 nM) in a total volume of 30 µl of binding buffer supplemented with bovine serum albumin and protease inhibitors. Total (no peptide added) and non-specific binding (defined using 10 µM α-cobratoxin) was determined in triplicate, for each concentration of each ligand. Following the initial incubation, 1 ml of isotonic binding buffer, supplemented with bovine serum albumin (0.1% (w/v)) was added to each tube and the incubation was continued for a further 2 min at 22 ºC. The previously-performed dissociation binding experiments indicated that this volumetric expansion step allows some of the non-specific radioligand binding to dissociate, but has no measurable effect on specific binding, increasing the signal : noise ratio of the binding assay. Binding reactions were then terminated by filtration, washed, and counted as described previously.

[^{125}I]α-CtxArIB[V11L;V16A] autoradiography, effect of α7 genotype.

The preceding experiments demonstrated that [^{125}I]α-CtxArIB[V11L;V16A] binding to mouse brain membranes was saturable, showed relatively rapid kinetics, and seemed to occur only at α7 nAChRs. To address this issue further, autoradiography was performed using sections from both wild-type and α7$^{-/-}$ mouse brains.

Autoradiographic procedures were similar to those described previously for [^{125}I]α-CtxMII (Whiteaker et al., 2000b). Before incubation with [$^{125}I_1$]α-CtxArIB[V11L;V16A] or [$^{125}I_2$]α-CtxArIB[V11L;V16A], four series of sections from each mouse were incubated in binding buffer (NaCl, 144 mM; KCl, 1.5 mM; $CaCl_2$, 2 mM; $MgSO_4$, 1 mM; HEPES, 20 mM; bovine serum albumin, 0.1% (w/v); pH = 7.5) + PMSF (1 mM, to inactivate endogenous serine proteases) at 22 °C for 15 min. For all binding reactions, the standard binding buffer was supplemented with bovine serum albumin (0.1% (w/v)), 5 mM EDTA, 5 mM EGTA, and 10 µg / ml each of aprotinin, leupeptin trifluoroacetate, and pepstatin A to protect the ligand from endogenous proteases. A series of sections was then incubated with 1 nM [$^{125}I_1$]α-CtxArIB[V11L;V16A] for 2h at 22°C, while a second series was incubated under the same conditions with 1 nM [$^{125}I_2$]α-CtxArIB[V11L;V16A]. The remaining series were then used to determine non-specific labeling by the two radioligands, in the presence of 10 µM α-cobratoxin. Following incubation, the slides were washed as follows: 30 sec in binding buffer + 0.1% (w/v) bovine serum albumin (22 °C), 30 sec in binding buffer + 0.1% (w/v) bovine serum albumin (0 °C), 5 sec in 0.1x binding buffer + 0.01% (w/v) bovine serum albumin (twice at 0 °C), and twice at 0 °C for 5 sec in 5 mM HEPES (pH = 7.5).

Sections were initially dried with a stream of air, then by overnight storage (22 °C) under vacuum before exposure to Super Resolution phosphorimaging screens (Perkin Elmer Life Sciences; Boston, MA; 2 – 4 d exposure) for image capture. Images were collected using a Packard Cyclone system (Perkin Elmer Life Sciences; Boston, MA).

[^{125}I]α-CtxArIB[V11L;V16A] lot lasting tests.

In order to test the stability of [$^{125}I_1$]α-CtxArIB[V11L;V16A] and [$^{125}I_2$]α-CtxArIB[V11L;V16A], saturation binding parameters were measured in a series of

JPET Fast Forward. Published on March 6, 2008 as DOI: 10.1124/jpet.108.136895
This article has not been copyedited and formatted. The final version may differ from this version.

assays performed at weekly intervals. At each time point, for each radioligand, peak signal : noise ratio, binding affinity (K_d), and maximum binding (B_{max}) were measured. Saturation binding assays were performed as described previously for hippocampal membranes, but using midbrain membranes. Midbrain tissue was used in this case since this is a large brain region (providing sufficient tissue for this extended series of experiments) and contains a moderate density of α7 nAChRs, permitting the collection of large (in terms of absolute counts) amounts of both specific and non-specific binding from the same samples. In contrast, hippocampal membranes yielded very few non-specific counts at very low ligand concentrations, making accurate determination of the non-specific signal difficult.

[I_1]α-CtxArIB[V11L;V16A] nAChR subtype selectivity tests.

It was apparent from the preceding autoradiographic experiments that moderate concentrations of [$^{125}I_1$]α-CtxArIB[V11L;V16A] only bind to α7 nAChRs. However, it was still necessary to investigate whether iodination resulted in increased affinity for non-α7 nAChR subtypes. According, the affinity of [I_1]α-CtxArIB[V11L;V16A] at native muscle (α1β1γδ), and neuronal (α4β2*, α6β2*, and β4*) subtype nAChRs was assessed using a series of inhibition binding assays. In addition, functional IC_{50} was measured at α9α10 nAChRs heterologously expressed in *Xenopus* oocytes (since no well-characterized native source of this nAChR subtype was available to us in a form that could be used for inhibition binding assays).

Inhibition of [^{125}I]α-Bgt binding to *Torpedo* membranes was used to measure the affinity of α-CtxArIB[V11L;V16A] and its derivatives for muscle-type α1β1γδ nAChRs. Identical assay conditions were used as those described for [^{125}I]α-Bgt binding to hippocampal membranes.

JPET Fast Forward. Published on March 6, 2008 as DOI: 10.1124/jpet.108.136895
This article has not been copyedited and formatted. The final version may differ from this version.

The interaction between α-CtxArIB[V11L;V16A] and its derivatives and α4β2* nAChRs was probed using displacement of [^{3}H]cytisine (5 nM, 21.2 Ci mmol^{-1}; Perkin Elmer, Boston, MA) binding to mouse thalamic membrane preparations. Incubations were performed at 22 ºC for 1 h in polystyrene 96-well plates. A total volume of 100 µl of isotonic binding buffer supplemented with protease inhibitors was used for incubations. α-CtxArIB[V11L;V16A] concentrations of 0.3 nM – 10 µM were used, and blanks were defined using 100 µM (-)-nicotine tartrate. Binding reactions were terminated by filtration onto single layers of Inotech 0.75 µm retention glass fiber filters that were soaked in 0.5% polyethylenimine for [^{3}H]cytisine assays. Samples were washed as described for [^{125}I]α-Bgt binding. Following addition of 1 ml of Budget Solve Scintillation Fluid (Research Products International, Mount Prospect, IL) to each sample, bound radioligand was quantitated by liquid scintillation counting (at 45% efficiency), using a Packard 1600 TR Liquid Scintillation Spectrometer.

Affinity for [^{125}I]α-CtxMII-binding nAChRs (α6β2* subtype (Gotti et al., 2005); was assessed using pooled membranes from mouse olfactory tubercle, striatum, and superior colliculus. The conditions were the same as described in Salminen et al. (2005) and very similar to those described previously for [^{125}I]α-Bgt binding, with the following modifications. [^{125}I]α-CtxMII (2200 Ci mmol^{-1}) was used at 0.5 nM, initial incubations proceeded for 2 h, and incubations were continued for 4 min after the dilution step. Bound radioligand was quantitated by gamma counting, as described previously.

The affinity of α-CtxArIB[V11L;V16A] for native β4* nAChRs was measured using inhibition of [^{125}I]epibatidine (200 pM; 2200 Ci mmol^{-1}; Perkin Elmer, Boston, MA) binding in the presence of the β2* nAChR-selective agonist A85380 (10 nM, unlabeled), as described in (Whiteaker et al., 2000a). The inferior colliculus, interpeduncular nucleus, medial habenula, and olfactory bulbs contain relatively high proportions of β4* nAChRs

JPET Fast Forward. Published on March 6, 2008 as DOI: 10.1124/jpet.108.136895
This article has not been copyedited and formatted. The final version may differ from this version.

when compared to other brain regions (Whiteaker et al., 2000a), so membranes from these regions were used in the present study. A total incubation volume of 30 µl of isotonic binding buffer supplemented with protease inhibitors was used, and incubations proceeded at 22 ºC for 2 h in polystyrene 96-well plates. Non-specific binding was again defined in the presence of 100 µM (-)-nicotine tartrate, and binding reactions were terminated and washed as described for [^{3}H]cytisine, previously.

Finally, the affinity of α-CtxArIB[V11L; V16A] for α9α10 nAChRs was measured using inhibition of [^{125}I]epibatidine (5 nM) binding to transfected *Xenopus* oocyte membranes. The specific activity of commercially-available [^{125}I]epibatidine (Perkin Elmer, Boston, MA) was reduced 10-fold (to 220 Ci mmol^{-1}) by isotopic dilution with non-radioactive iodoepibatidine (a kind gift of K.J. Kellar, Georgetown University, Washington D.C.). The total incubation volume was 30 µl using isotonic binding buffer supplemented with protease inhibitors and PMSF (0.1 mM). Incubations proceeded at 22 ºC for 1 h in polystyrene 96-well plates. Non-specific binding was defined in the presence of 1 µM unlabeled α-Bgt, and binding reactions were terminated and washed as described for [^{125}I]epibatidine, previously.

Data analysis.

A more detailed account of how the data analysis was performed is given in the Supplemental Data section. Since much of the analysis was performed using standard models, these equations are not given here but are provided in the Supplemental Data for readers who wish to follow our approach more thoroughly. A less commonly-used approach was employed to determine the signal : noise ratio of the ligand binding assays, and this is presented in full here.

For binding association kinetics, data were fit to a single exponential increase to maximum model (Equation 1, Supplemental Figure 1), providing an observed (apparent)

JPET Fast Forward. Published on March 6, 2008 as DOI: 10.1124/jpet.108.136895
This article has not been copyedited and formatted. The final version may differ from this version.

association rate. For binding dissociation kinetics, data were fit to a single exponential decrease model (Equation 2, Supplemental Figure 1). These kinetic parameters were also used, together with the ligand concentration used, to calculate K_d values for binding as the quotient of the apparent association and dissociation rates (Equation 3, Supplemental Figure 1).

Saturation of specific binding was fit using the Hill equation (Equation 4, Supplemental Figure 1), while non-specific binding was modeled as a linear increase with ligand concentration (Equation 5, Supplemental Figure 1). Combining these representations allowed the signal: noise (specific: non-specific binding) ratio to be described:

$$\text{signal} : \text{noise} = \frac{B_{max}[L]^{n_H}}{(m[L] + c)(K_d{}^{n_H} + [L]^{n_H})} \qquad \text{Equation 6}$$

where B_{max} is specific binding at saturation, [L] is the ligand concentration, n_H is the Hill coefficient of specific binding, K_d is the affinity constant of specific binding, m is the slope of increasing non-specific binding as ligand concentration [L] increases, and c is non-specific binding at [L] = 0 (counter background).

Differentiation of Equation 1 in terms of x gives Equation 7:

$$\frac{\partial}{\partial x}(\text{signal} : \text{noise}) = \frac{B_{max}[L]^{n_H-1}(cn_H K_d{}^{n_H} + m[L](K_d{}^{n_H}(n_H - 1) - [L]^{n_H}))}{(m[L] + c)^2 (K_d{}^{n_H} + [L]^{n_H})^2} \qquad \text{Equation 7}$$

The value of Equation 7 is zero at the value of [L] corresponding to peak signal : noise ratio. This value of [L] was determined for individual experiments by least-squares data fitting of Equation 7 using the parameters previously obtained from fitting specific binding to the Hill equation and non-specific binding to a simple linear increase with concentration. In turn, the peak signal : noise ratios for individual experiments were then calculated by entering the relevant value of [L] into Equation 6.

Data fits were performed using non-linear, least-squares curve fitting in SigmaPlot V9.0.1 Statistical analysis (t-tests, ANOVA) was performed using SPSS V15.0.1. Both software packages were purchased from Systat Software Inc., Point Richmond, CA.

JPET Fast Forward. Published on March 6, 2008 as DOI: 10.1124/jpet.108.136895
This article has not been copyedited and formatted. The final version may differ from this version.

RESULTS:

Effects of α-CtxArIB[V11L;V16A] His-iodination.

Both mono- and diiodinated α-CtxArIB[V11L;V16A] derivatives were generated using non-radioactive iodination at the parent compound's single histidine residue. This allowed the effects of iodination on α-CtxArIB[V11L;V16A] affinity for α7 nAChRs to be assessed. Iodinated products were HPLC purified (Supplemental Figure 2) and toxin iodination was confirmed with matrix assisted laser desorption time-of-flight mass spectrometry. The monoisotopic masses (in Daltons) were: monoiodo peptide, 2436.88 calculated, 2436.8 observed; diodo peptide, 2562.78 calculated, 2562.8 observed. As shown in Figure 1, histidine iodination mildly increased affinity at α7 nAChRs as measured by inhibition of [$^{125}I_1$]α-Bgt (high specific activity, monoiodinated α-Bgt) binding to mouse hippocampal membranes. This increase in affinity appeared to be progressive, and the diiodo derivative had significantly higher affinity for α7 nAChRs than did the parent compound (see figure legend for statistics). These K_i values may be marginally higher than would be predicted from functional data (α-CtxArIB[V11L;V16A] functional IC_{50} = 0.356 nM, corresponding to a predicted binding K_i value of 2.25 nM (Whiteaker et al., 2007), compared to 10.5 nM as measured here). This presumably reflects the effects of [^{125}I]α-Bgt's exceptionally slow dissociation kinetics, which make measuring true equilibrium affinity constants impossible.

[^{125}I]α-CtxArIB[V11L;V16A] association and dissociation kinetics.

In light of the promising data from the cold-iodinated α-CtxArIB[V11L;V16A] derivatives, attempts were made to identify highly α7 nAChR-selective [^{125}I]α-CtxArIB[V11L;V16A] binding using both the mono- ([$^{125}I_1$]α-CtxArIB[V11L;V16A]) and diiodinated ([$^{125}I_2$]α-CtxArIB[V11L;V16A]) versions of this potential ligand. As shown in

JPET Fast Forward. Published on March 6, 2008 as DOI: 10.1124/jpet.108.136895
This article has not been copyedited and formatted. The final version may differ from this version.

Figure 2, specific labeling of mouse hippocampal membranes was seen. Association was described well by a single exponential increase, and was essentially complete after 120 – 180 min at 22 ºC (Figure 2, panel A). Observed association rates for the mono- and diiodinated forms were indistinguishable (monoiodo k_{obs} = 0.027 ± 0.007 min^{-1}; diiodo k_{obs} = 0.019 ± 0.003 min^{-1}; see figure legend for detailed statistics). Dissociation of [^{125}I]α-CtxArIB[V11L;V16A] also could be fit with a single exponential model (Figure 2, panel B), and was again nearly complete after 180 min at 22 ºC. In this case, dissociation of the monoiodo derivative was significantly faster (k_{off} = 0.0195 ± 0.0008 min^{-1}) than that of the diiodo peptide (0.0115 ± 0.0010 min^{-1}; p = 0.0039, statistics in figure legend). When these kinetic constants were used to calculate K_d values (see Methods section), results of 2.67 nM for [$^{125}I_1$]α-CtxArIB[V11L;V16A] and 1.51 nM for [$^{125}I_2$]α-CtxArIB[V11L;V16A] were obtained. The higher affinity of the diiodo peptide is thus almost entirely due to its slower dissociation.

[^{125}I]α-CtxArIB[V11L;V16A] saturation binding.

Next, we measured the performance of both [^{125}I]α-CtxArIB[V11L;V16A] derivatives in saturation binding assays, again using mouse hippocampal membranes as a source of α7 nAChRs. Saturation binding was also performed for [$^{125}I_1$]α-Bgt, to provide a comparison between this classical α7-directed ligand and the novel α-CtxArIB derivatives. Total and non-specific binding for each of the ligands are shown in Figure 3 (panel A). As may be seen, [$^{125}I_1$]α-Bgt produced the greatest amount of non-specific binding at any given ligand concentration, followed by [$^{125}I_2$]α-CtxArIB[V11L;V16A] and then [$^{125}I_1$]α-CtxArIB[V11L;V16A]. Specific binding was calculated for each ligand, and was saturable as shown in Figure 3 (panel B). The density of binding sites was indistinguishable between the three ligands (B_{max} = 72.7 ± 6.8, 70.0 ± 4.0, and 69.7 ± 5.2

JPET Fast Forward. Published on March 6, 2008 as DOI: 10.1124/jpet.108.136895
This article has not been copyedited and formatted. The final version may differ from this version.

fmol mg^{-1} for [$^{125}I_1$]α-CtxArIB[V11L;V16A], [$^{125}I_2$]α-CtxArIB[V11L;V16A] and [$^{125}I_1$]α-Bgt, respectively). In contrast, specific [$^{125}I_1$]α-Bgt binding had slightly (although significantly) higher measured affinity (K_d = 0.52 ± 0.16 nM) than either of the two [^{125}I]α-CtxArIB[V11L;V16A] derivatives (K_d = 1.15 ± 0.13 and 0.93 ± 0.13 nM; respectively; see figure legend for statistics). Finally, the ratio of specific to nonspecific binding was calculated at each concentration of each ligand, as shown in panel C of figure 3. Peak signal : noise ratios were similar for each ligand (6.21 ± 0.52 : 1, 4.88 ± 0.19 : 1, and 5.79 ± 2.52 : 1 for [$^{125}I_1$]α-CtxArIB[V11L;V16A], [$^{125}I_2$]α-CtxArIB[V11L;V16A] and [$^{125}I_1$]α-Bgt, respectively), as were the concentrations at which these peaks occurred (0.51 ± 0.19, 0.38 ± 0.05, and 0.29 ± 0.08 for [$^{125}I_1$]α-CtxArIB[V11L;V16A], [$^{125}I_2$]α-CtxArIB[V11L;V16A] and [$^{125}I_1$]α-Bgt, respectively). Neither the peak signal : noise ratio nor the concentration at which this peak occurred were statistically distinguishable between the three peptides (see figure legend for details).

[^{125}I]α-CtxArIB[V11L;V16A] autoradiography, effect of α7 genotype.

The previous experiments demonstrated that [^{125}I]α-CtxArIB[V11L;V16A] binding to mouse brain membranes was both saturable and showed relatively rapid kinetics. The inhibition binding experiments also seemed to indicate that iodinated α-CtxArIB[V11L;V16A] derivatives retained the parent compound's ability to discriminate α7 from other nAChR subtypes. However, it was a remote possibility that [^{125}I]α-CtxArIB[V11L;V16A] might also label non-nAChR targets. To address this issue, autoradiography was performed using sections from both wild-type and $\alpha7^{-/-}$ mouse brains. An example is shown in Figure 4, at the level of the hippocampus. In wild-type sections, the binding pattern (layered cortical binding, and intense labeling of hypothalamic nuclei, amygdala, and hippocampus) was typical of α7-specific nAChR

JPET Fast Forward. Published on March 6, 2008 as DOI: 10.1124/jpet.108.136895
This article has not been copyedited and formatted. The final version may differ from this version.

labeling in mouse brain sections, as previously shown using [^{125}I]α-Bgt (Franceschini et al, 2002). As would be expected, given the greater specific activity of [$^{125}I_2$]α-CtxArIB[V11L;V16A] compared to [$^{125}I_1$]α-CtxArIB[V11L;V16A], the labeling was more intense with the former ligand. For both ligands, deletion of the nAChR α7 gene resulted in the complete loss of specific labeling across all brain regions (above a low, even, level of non-specific binding).

[^{125}I]α-CtxArIB[V11L;V16A] lot lasting tests.

The rates of deterioration of [$^{125}I_1$]α-CtxArIB[V11L;V16A] and [$^{125}I_2$]α-CtxArIB[V11L;V16A] were monitored using saturation binding experiments, performed at weekly intervals. The following parameters were measured at each time point, for each radioligand: peak signal : noise ratio, binding affinity (K_d), and maximum binding (B_{max}).

As illustrated in figure 5, these parameters were most stable for [$^{125}I_1$]α-CtxArIB[V11L;V16A]. Both radioligands exhibited a drop in signal : noise performance over the time period investigated (12 weeks; see panel A, Figure 5), but for [$^{125}I_1$]α-CtxArIB[V11L;V16A] performance only deteriorated significantly vs. initial levels in weeks 10-12. In contrast, [$^{125}I_2$]α-CtxArIB[V11L;V16A] suffered from a significant loss of performance vs. initial levels beginning in week 3, and suffered further deterioration in the following weeks. For both ligands, the deterioration of signal : noise ratio was fit well using a single exponential decay model. The decay rate for [$^{125}I_2$]α-CtxArIB[V11L;V16A] signal : noise ratio (0.200 wk^{-1}) was approximately 2.5 times faster than that for [$^{125}I_1$]α-CtxArIB[V11L;V16A] (0.0761 wk^{-1}).

In contrast, little change in affinity was seen for either ligand during extended testing (Figure 5, panel B), with [$^{125}I_1$]α-CtxArIB[V11L;V16A] K_d values remaining essentially constant throughout the 12 week investigation. The K_d values measured for

JPET Fast Forward. Published on March 6, 2008 as DOI: 10.1124/jpet.108.136895
This article has not been copyedited and formatted. The final version may differ from this version.

[$^{125}I_2$]α-CtxArIB[V11L;V16A] showed an upwards trend (apparent lowering of affinity) with time, but this never reached significance. To some extent, this lack of significance may reflect the difficulty of measuring accurate K_d values at later time points, due to deteriorating assay performance. In any case, apparent changes in K_d values were less dramatic than those seen for signal : noise ratio.

Maximum binding (B_{max}) measured using [$^{125}I_1$]α-CtxArIB[V11L;V16A] saturation binding remained similar, even after 12 weeks. (Figure 5, panel C). In contrast a slight, but significant decrease in apparent B_{max} was observed when using [$^{125}I_2$]α-CtxArIB[V11L;V16A], with values in weeks 10 – 12 being lower than in week 1.

[I]α-CtxArIB[V11L;V16A] affinity at non-α7 nAChR subtypes.

The affinity of iodinated α-CtxArIB[V11L;V16A] derivatives was also tested at non-α7 nAChR subtypes, to determine if they retained the α7 nAChR selectivity of the non-iodinated parent compound. As shown in Figure 6, iodinated derivatives of α-CtxArIB[V11L;V16A] did not significantly inhibit binding at a wide variety of other known nAChR subtypes, including several that also bind α-Bgt or MLA with high affinity. There may have been some slight inhibition of binding to α6β2* and α9α10 nAChRs at very high (μM) concentrations, but both [I]α-CtxArIB[V11L;V16A] derivatives retain a > 100-fold preference for α7 over α6β2* and α9α10 nAChRs, making them highly selective ligands.

JPET Fast Forward. Published on March 6, 2008 as DOI: 10.1124/jpet.108.136895
This article has not been copyedited and formatted. The final version may differ from this version.

DISCUSSION:

As outlined in the Introduction [^{125}I]α-Bgt, while a useful and informative tool, suffers from significant problems of specificity when used outside of the mammalian CNS, and exceptionally slow kinetics. In this series of studies, we describe the synthesis and characterization of mono- and diiodinated versions of CtxArIB[V11L;V16A]. These conotoxin derivatives, particularly [$^{125}I_1$]CtxArIB[V11L;V16A], address the problems associated with the use of [^{125}I]α-Bgt, providing greater specificity and much faster kinetics.

Earlier studies had provided two highly α7-selective (> 300-fold vs. other nAChR subtypes) derivatives of CtxArIB as potential lead compounds (α-CtxArIB[V11L;V16A] and α-CtxArIB[V11L;V16D]; (Whiteaker et al, 2007)). We chose the former on the basis of its higher α7 affinity (0.36 nM *vs*. 1.09 nM IC_{50} vs. α7 nAChR function; (Whiteaker et al, 2007)), which would reduce the potential impact of any iodination-induced affinity loss. All of the α-CtxArIB derivatives that we had previously characterized contained a single histidine residue at position 15 (H15), providing a single site for iodination. This is in contrast to α-CtxMII, which hosts two naturally-occurring histidines. Thus, histidine iodination of α-CtxMII would produce a confusing mix of iodination products (a problem solved by addition of an N-terminal tyrosine and selective iodination at this newly-introduced residue; (Whiteaker et al, 2000b)). Initial concerns that iodination at H15 would result in a loss of α7 affinity proved unfounded. In fact, iodination at this position mildly increased affinity for α7 nAChRs, with a progressive increase in affinity from unlabeled through monoiodinated to diiodinated H15 α-CtxArIB[V11L;V16A]. Since addition of bulky, relatively non-polar iodine atom(s) at the H15 position was well-tolerated (or even advantageous), this site may be suitable for the introduction of substituents with similar properties (photoactivatable or fluorescent labels, biotin).

JPET Fast Forward. Published on March 6, 2008 as DOI: 10.1124/jpet.108.136895
This article has not been copyedited and formatted. The final version may differ from this version.

Kinetics experiments illustrated a further advantage of [^{125}I]α-CtxArIB[V11L;V16A] over [^{125}I]α-Bgt, that of relatively rapid association and dissociation. The dissociation rate of [^{125}I]α-Bgt from α7 nAChRs has been measured as 0.00074 min^{-1} at 20 ºC (Salvaterra and Mahler, 1976), which is approximately 26 and 16 times slower than the rates measured for [$^{125}I_1$]α-CtxArIB[V11L;V16A] and [$^{125}I_2$]α-CtxArIB[V11L;V16A], respectively. In contrast, the true association rates (k_{on}) of both [^{125}I]α-CtxArIB[V11L;V16A] ligands were measured as 7.5 x 10^6 M^{-1} min^{-1}, which is only 3.3x faster than that reported for the association of [^{125}I]α-Bgt to α7 nAChRs (2.3 x 10^6 M^{-1} min^{-1}; (Salvaterra and Mahler, 1976)). In practical terms, the faster dissociation of [^{125}I]α-CtxArIB[V11L;V16A] compared to [^{125}I]α-Bgt is largely responsible for the lower α7 nAChR affinity of [^{125}I]α-CtxArIB[V11L;V16A] derivatives compared to [^{125}I]α-Bgt, and makes equilibrium binding assays with [^{125}I]α-CtxArIB[V11L;V16A] derivatives feasible. The benefits of being able to perform true equilibrium binding assays can be seen when comparing the K_i values calculated for [I]α-CtxArIB[V11L;V16A] derivatives using [^{125}I]α-Bgt inhibition binding (4.92 ± 2.32 nM and 1.96 ± 0.43 nM for mono- and diiodo derivatives, respectively) to the K_d values observed from direct [^{125}I]α-CtxArIB[V11L;V16A] saturation binding (1.15 ± 0.13 nM and 0.93 ± 0.13 nM respectively). The saturation binding values are closer to those calculated using kinetic analysis (2.67 nM and 1.51 nM).

In hippocampal saturation binding experiments [$^{125}I_1$]α-CtxArIB[V11L;V16A], [$^{125}I_2$]α-CtxArIB[V11L;V16A], and [$^{125}I_1$]α-Bgt all bound to the same number of sites, as would be expected if each ligand was binding specifically to a single nAChR population (α7 nAChRs in this case). The saturation binding experiments also showed that both [$^{125}I_1$]α-CtxArIB[V11L;V16A] and [$^{125}I_2$]α-CtxArIB[V11L;V16A] have lower non-specific binding than [$^{125}I_1$]α-Bgt at equivalent concentrations (with [$^{125}I_1$]α-CtxArIB[V11L;V16A]

JPET Fast Forward. Published on March 6, 2008 as DOI: 10.1124/jpet.108.136895
This article has not been copyedited and formatted. The final version may differ from this version.

appearing the cleanest-binding of all in this comparison). Despite this, maximum signal : noise ratios were similar for each radioligand, with increased non-specific binding being approximately cancelled out by higher affinity along the series [$^{125}I_1$]α-CtxArIB[V11L;V16A] to [$^{125}I_2$]α-CtxArIB[V11L;V16A] to [$^{125}I_1$]α-Bgt. Thus, the real-world assay performance of each of these radioligands (when newly synthesized) is very similar.

As assessed by α7 affinity, binding kinetics, and assay performance, the two [^{125}I]α-CtxArIB[V11L;V16A] derivatives are quite similar to each other when newly synthesized. However, significant differences were uncovered when the deterioration of [$^{125}I_1$]α-CtxArIB[V11L;V16A] and [$^{125}I_2$]α-CtxArIB[V11L;V16A] lots was compared. From this point of view [$^{125}I_1$]α-CtxArIB[V11L;V16A] is clearly a better radioligand since its signal : noise ratio performance drops more slowly and no changes in B_{max} or K_d were measured over a 12 week period, in contrast to the situation with [$^{125}I_2$]α-CtxArIB[V11L;V16A]. Nevertheless, in certain well-defined circumstances (very low α7 nAChR expression where extremely high specific activity would be needed to obtain a measurable signal, and when the radioligand could be used within two weeks of being synthesized), [$^{125}I_2$]α-CtxArIB[V11L;V16A] could be a very useful alternative to [$^{125}I_1$]α-CtxArIB[V11L;V16A]. It is not known exactly why [$^{125}I_2$]α-CtxArIB[V11L;V16A] undergoes more-rapid and more-extensive deterioration than does [$^{125}I_1$]α-CtxArIB[V11L;V16A]. Part of the explanation may simply be the higher radioactive concentration and thus radiolysis rate in the [$^{125}I_2$]α-CtxArIB[V11L;V16A] solution (both peptides were stored at similar concentrations, giving the [$^{125}I_2$]α-CtxArIB[V11L;V16A] stock approximately double the radioactive concentration compared to the [$^{125}I_1$]α-CtxArIB[V11L;V16A] stock). Additionally, studies of diiodo-insulin illustrate a further mechanism by which the assay performance of diiodo peptides may suffer rapid deterioration. Decay of the first

radioiodine on diiodo-insulin molecules results in a mix of decay products, including free radioiodide and radiolabeled polymers that exhibit low receptor affinity and high non-specific binding (Maceda et al., 1982). Accumulation of either or both of these products could be responsible for the relatively rapid deterioration of [$^{125}I_2$]α-CtxArIB[V11L;V16A] samples seen in this study.

It was also possible that iodination of α-CtxArIB[V11L;V16A] could result in a loss of the parent compound's selective interaction with α7 nAChRs. Again, this concern proved unfounded, as assessed using two separate approaches. First, as illustrated in Fig 6, the mono-iodinated α-CtxArIB[V11L;V16A] derivative failed to interact with other nAChR subtypes (α1β1γδ, α4β2*, α6β2*, β4*, α9α10) with anything like the same affinity seen at α7 nAChRs. Second, all [^{125}I]α-CtxArIB[V11L;V16A] binding to mouse brain sections was abolished by nAChR α7 gene deletion. Thus, both the mono- and diiodo versions of [^{125}I]α-CtxArIB[V11L;V16A] retain the exceptional α7 selectivity of the parent compound, which is greater than that of α-Bgt.

References:

Baker ER, Zwart R, Sher E, and Millar NS (2004) Pharmacological properties of α9 α10 nicotinic acetylcholine receptors revealed by heterologous expression of subunit chimeras. *Molecular Pharmacology* **65**:453-460.

Changeux JP, Kasai M, and Lee CY (1970) Use of A Snake Venom Toxin to Characterize Cholinergic Receptor Protein. *Proceedings of the National Academy of Sciences of the United States of America* **67**:1241-&.

Chen DN and Patrick JW (1997) The alpha-bungarotoxin-binding nicotinic acetylcholine receptor from rat brain contains only the α7 subunit. *Journal of Biological Chemistry* **272**:24024-24029.

Clarke PBS (1992) The Fall and Rise of Neuronal Alpha-Bungarotoxin Binding-Proteins. *Trends in Pharmacological Sciences* **13**:407-413.

Clarke PBS, Schwartz RD, Paul SM, Pert CB, and Pert A (1985) Nicotinic Binding in Rat-Brain - Autoradiographic Comparison of [^{3}H]Acetylcholine, [^{3}H]Nicotine, and [^{125}I]α-Bungarotoxin. *Journal of Neuroscience* **5**:1307-1315.

Davies ARL, Hardick DJ, Blagbrough IS, Potter BVL, Wolstenholme AJ, and Wonnacott S (1999) Characterisation of the binding of [^{3}H]methyllycaconitine: a new radioligand for labelling α7-type neuronal nicotinic acetylcholine receptors. *Neuropharmacology* **38**:679-690.

Elgoyhen AB, Vetter DE, Katz E, Rothlin CV, Heinemann SF, and Boulter J (2001) α10: A determinant of nicotinic cholinergic receptor function in mammalian vestibular and

cochlear mechanosensory hair cells. *Proceedings of the National Academy of Sciences of the United States of America* **98**:3501-3506.

Franceschini D, Paylor R, Broide R, Salas R, Bassetto L, Gotti C, and De Biasi M (2002) Absence of alpha 7-containing neuronal nicotinic acetylcholine receptors does not prevent nicotine-induced seizures. *Molecular Brain Research* **98**:29-40.

Gotti C, Hanke W, Maury K, Moretti M, Ballivet M, Clementi F, and Bertrand D (1994) Pharmacology and Biophysical Properties of α7 and α7-α-8 Alpha-Bungarotoxin Receptor Subtypes Immunopurified from the Chick Optic Lobe. *European Journal of Neuroscience* **6**:1281-1291.

Gotti C, Moretti M, Clementi F, Riganti L, McIntosh JM, Collins AC, Marks MJ, and Whiteaker P (2005) Expression of nigrostriatal α6-containing nicotinic acetylcholine receptors is selectively reduced, but not eliminated, by β3 subunit gene deletion. *Molecular Pharmacology* **67**:2007-2015.

Haberberger RV, Bernardini N, Kress M, Hartmann P, Lips KS, and Kummer W (2004) Nicotinic acetylcholine receptor subtypes in nociceptive dorsal root ganglion neurons of the adult rat. *Autonomic Neuroscience-Basic & Clinical* **113**:32-42.

Maceda BP, Linde S, Sonne O, and Gliemann J (1982) [^{125}I]-Labeled Diiodoinsulins - Binding Affinities, Biologic Potencies, and Properties of Their Decay Products. *Diabetes* **31**:634-640.

Marks MJ, Smith KW, and Collins AC (1998) Differential agonist inhibition identifies multiple epibatidine binding sites in mouse brain. *Journal of Pharmacology and Experimental Therapeutics* **285**:377-386.

Martyn JAJ and Richtsfeld M (2006) Succinylcholine-induced hyperkalemia in acquired pathologic states - Etiologic factors and molecular mechanisms. *Anesthesiology* **104**:158-169.

Morley BJ, Li HS, Hiel H, Drescher DG, and Elgoyhen AB (1998) Identification of the subunits of the nicotinic cholinergic receptors in the rat cochlea using RT-PCR and in situ hybridization. *Molecular Brain Research* **53**:78-87.

Nguyen VT, Ndoye A, and Grando SA (2000) Novel human α9 acetylcholine receptor regulating keratinocyte adhesion is targeted by pemphigus vulgaris autoimmunity. *American Journal of Pathology* **157**:1377-1391.

Parker MJ, Beck A, and Luetje CW (1998) Neuronal Nicotinic Receptor β2 and β4 Subunits Confer Large Differences in Agonist Binding Affinity. *Molecular Pharmacology* **54**:1132-1139.

Pauly JR, Stitzel JA, Marks MJ, and Collins AC (1989) An Autoradiographic Analysis of Cholinergic Receptors in Mouse-Brain. *Brain Research Bulletin* **22**:453-459.

Peng HS, Ferris RL, Matthews T, Hiel H, Lopez-Albaitero A, and Lustig LR (2004) Characterization of the human nicotinic acetylcholine receptor subunit α9 (CHRNA9) and α10 (CHRNAIO) in lymphocytes. *Life Sciences* **76**:263-280.

Quik M, Sum JD, Whiteaker P, McCallum SE, Marks MJ, Musachio J, McIntosh JM, Collins AC, and Grady SR (2003) Differential declines in striatal nicotinic receptor subtype function after nigrostriatal damage in mice. *Molecular Pharmacology* **63**:1169-1179.

Salminen O, Whiteaker P, Grady SR, Collins AC, McIntosh JM, and Marks MJ (2005) The subunit composition and pharmacology of α-conotoxin MII-binding nicotinic acetylcholine receptors studied by a novel membrane-binding assay. *Neuropharmacology* **48**:696-705.

Salvaterra PM and Mahler HR (1976) Nicotinic Acetylcholine-Receptor from Rat-Brain - Solubilization, Partial-Purification, and Characterization. *Journal of Biological Chemistry* **251**:6327-6334.

Whiteaker P, Christensen S, Yoshikami D, Dowell C, Watkins M, Gulyas J, Rivier J, Olivera BM, and McIntosh JM (2007) Discovery, Synthesis, and Structure Activity of a Highly Selective α7 Nicotinic Acetylcholine Receptor Antagonist. *Biochemistry* **46**:6628-6638.

Whiteaker P, Jimenez M, McIntosh JM, Collins AC, and Marks MJ (2000a) Identification of a novel nicotinic binding site in mouse brain using [^{125}I]-epibatidine. *British Journal of Pharmacology* **131**:729-739.

Whiteaker P, McIntosh JM, Luo SQ, Collins AC, and Marks MJ (2000b) ^{125}I-alpha-conotoxin MII identifies a novel nicotinic acetylcholine receptor population in mouse brain. *Molecular Pharmacology* **57**:913-925.

FOOTNOTES:

This work was supported by NIH grants DA12242 (to P.W.), MH 53631 and GM 48677 (to J.M.M.), and DA-15663 (to A.C.C.). We thank J.E. Rivier and R. Kaiser of the Salk Institute, La Jolla, CA for assistance with mass spectrometry.

JPET Fast Forward. Published on March 6, 2008 as DOI: 10.1124/jpet.108.136895
This article has not been copyedited and formatted. The final version may differ from this version.

Legends for Figures:

Figure 1: Effects of α-CtxArIB[V11L;V16A] His-iodination.

Non-radioactive mono- and diiodinated derivatives were generated by cold-iodination at H15 of α-CtxArIB[V11L;V16A]. Peptides were tested for their ability to inhibit [$^{125}I_1$]α-Bgt (2 nM) binding to hippocampal membranes. Affinity values were: native K_i = 10.5 ± 2.19 nM (filled squares), monoiodo K_i = 4.92 ± 2.32 nM (hollow circles); diiodo K_i = 1.96 ± 0.43 nM (filled circles); n = 3 in each case. One way ANOVA indicated that diiodo α-CtxArIB[V11L;V16A] had significantly higher α7 nAChR potency than the parent peptide ($F_{[2,6]}$ = 5.48, p = 0.044). Lines were generated by non-linear least-squares curve-fitting. r^2 values were 0.996, 0.999, and 0.989 for the summary fits to data from native, monoiodo, and diiodo peptides, respectively.

Figure 2: [^{125}I]α-CtxArIB[V11L;V16A] association and dissociation kinetics.

The association and dissociation time-courses of specific [$^{125}I_1$]α-CtxArIB[V11L;V16A] and [$^{125}I_2$]α-CtxArIB[V11L;V16A] (1 nM in each case) labeling of hippocampal membranes were observed at 22 ºC. Panel A., association kinetics. Equilibrium binding (B_{max}) was measured for both radioligands, and was statistically identical (B_{max} monoiodo = 22.5 ± 3.4 fmol mg^{-1} (protein), diiodo = 24.1 ± 2.0 fmol mg^{-1}; n = 3 for both, p = 0.75 by t-test). Observed association rates (k_{obs}) were also indistinguishable (k_{obs} monoiodo = 0.027 ± 0.007 min^{-1}, diiodo = 0.019 ± 0.003 min^{-1}; n = 3 for both, p = 0.33 by t-test). Lines were generated by non-linear least-squares curve-fitting. r^2 values were 0.989, and 0.976 for the summary fits to data from monoiodo and diiodo peptides, respectively. Panel B., dissociation kinetics. Initial binding (B_o) was measured for both radioligands, and was statistically identical (B_o monoiodo = 30.4 ± 1.5 fmol mg^{-1} (protein), diiodo = 31.1 ± 1.7 fmol mg^{-1}; n = 3 for both, p = 0.78 by t-test). Dissociation rates (k_{off}) were

JPET Fast Forward. Published on March 6, 2008 as DOI: 10.1124/jpet.108.136895
This article has not been copyedited and formatted. The final version may differ from this version.

significantly quicker for [$^{125}I_1$]- vs. [$^{125}I_2$]α-CtxArIB[V11L;V16A], however (k_{off} monoiodo = 0.020 ± 0.001 min^{-1}, diiodo = 0.0115 ± 0.003 min^{-1}; n = 3 for both, p = 0.0039 by t-test). Lines were generated by non-linear least-squares curve-fitting. r^2 values were 0.997, and 0.991 for the summary fits to data from monoiodo and diiodo peptides, respectively.

Figure 3: [^{125}I]α-CtxArIB[V11L;V16A] saturation binding.

Panel A., Total and non-specific binding to mouse hippocampal membranes was measured using a range of [^{125}I]α-CtxArIB[V11L;V16A] concentrations, and compared to that of [$^{125}I_1$]α-Bgt. Non-specific binding was defined by addition of 10 μM α-cobratoxin. Each point is the mean ± SEM of three individual determinations. Lines were generated by non-linear least-squares curve-fitting. For total binding, r^2 values were 0.999 for the summary fits for all three peptides tested. For non-specific binding, r^2 values were 0.992 for [$^{125}I_1$]α-CtxArIB[V11L;V16A] and 0.999 for the summary fits to data from [$^{125}I_2$]α-CtxArIB[V11L;V16A] and [$^{125}I_1$]α-Bgt. Panel B., Specific binding to mouse hippocampal membranes was determined as the difference between specific and non-specific binding for each radioligand. Binding parameters (B_{max}, n_H, and K_d) were calculated by fitting individual determinations to the Hill equation. B_{max} values were statistically identical for each compound (72.7 ± 6.8, 70.0 ± 4.0, 69.7 ± 14.0 fmol mg^{-1} (protein) for [$^{125}I_1$]α-CtxArIB[V11L;V16A], [$^{125}I_2$]α-CtxArIB[V11L;V16A], and [$^{125}I_1$]α-Bgt, respectively; mean ± SEM, n = 3; 1-way ANOVA gives F [2,6] = 0.031, p = 0.969), as were n_H values (1.03 ± 0.08, 1.14 ± 0.10, 1.23 ± 0.11; 1-way ANOVA gives F [2,6] = 1.11, p = 0.388). While the affinities of [$^{125}I_1$]α-CtxArIB[V11L;V16A] and [$^{125}I_2$]α-CtxArIB[V11L;V16A] specific binding to hippocampal membranes were indistinguishable from each other, that of [$^{125}I_1$]α-Bgt was significantly higher (K_d values 1.15 ± 0.13 nM, 0.93 ± 0.13 nM, and 0.52 ± 0.16 nM, respectively; 1-way ANOVA gives F [2,6] = 5.11, p = 0.045, Tukey HSD *post hoc* test

JPET Fast Forward. Published on March 6, 2008 as DOI: 10.1124/jpet.108.136895
This article has not been copyedited and formatted. The final version may differ from this version.

confirms that [$^{125}I_1$]α-Bgt K_d is lower). Lines were generated by non-linear least-squares curve-fitting. r^2 values were 0.999, 0.996, and 0.998 for the summary fits for [$^{125}I_1$]α-CtxArIB[V11L;V16A], [$^{125}I_2$]α-CtxArIB[V11L;V16A], and [$^{125}I_1$]α-Bgt, respectively. Panel C., Specific : non-specific ratios were also calculated for each compound, as described in the Methods section. Neither the ligand concentration at which peak signal : noise ratio occurred, nor the ratio itself differed significantly between the radioligands, as assessed by one-way ANOVA ($F_{[2,6]} = 0.904$, $p = 0.454$ and $F_{[2,6]} = 0.209$, $p = 0.817$, respectively). Lines were generated by non-linear least-squares curve-fitting. r^2 values were 0.971, 0.967, and 0.876 for the summary fits for [$^{125}I_1$]α-CtxArIB[V11L;V16A], [$^{125}I_2$]α-CtxArIB[V11L;V16A], and [$^{125}I_1$]α-Bgt, respectively.

Figure 4: [^{125}I]α-Bgt and [^{125}I]α-CtxArIB[V11L;V16A] autoradiography, effect of α7 genotype.

Autoradiography was performed using sections from both wild-type and $\alpha7^{-/-}$ mouse brains, for [^{125}I]α-Bgt (0.5 nM) and both [$^{125}I_1$]α-CtxArIB[V11L;V16A] and [$^{125}I_2$]α-CtxArIB[V11L;V16A] (1 nM). While the greater specific activity of [$^{125}I_2$]α-CtxArIB[V11L;V16A] compared to [$^{125}I_1$]α-CtxArIB[V11L;V16A] resulted in more intense labeling with the former ligand, the patterns of labeling for all three radioligands were extremely similar in wild-type sections (left column). In $\alpha7^{-/-}$ sections, in contrast, each radioligand produced only a low, uniform, non-specific binding pattern (right column). Abbreviations for brain regions: A, amygdala; Cx1, layer I of cortex; Cx6, Layer VI of cortex; Hp, Hippocampus; ZI, zona incerta.

Figure 5: [^{125}I]α-CtxArIB[V11L;V16A] lot lasting tests.

JPET Fast Forward. Published on March 6, 2008 as DOI: 10.1124/jpet.108.136895
This article has not been copyedited and formatted. The final version may differ from this version.

Saturation binding experiments were performed on mouse midbrain membranes at weekly intervals using [$^{125}I_1$]α-CtxArIB[V11L;V16A] and [$^{125}I_2$]α-CtxArIB[V11L;V16A]. At each time point, for each radioligand, peak signal : noise ratio, binding affinity (K_d), and maximum binding (B_{max}) were measured as described in the Methods section. All points represent the mean ± SEM of two separate determinations. Panel A., Signal : noise ratio deteriorated over time for both ligands. One-way ANOVA indicated that assay signal : noise ratio changed significantly over time. For [$^{125}I_1$]α-CtxArIB[V11L;V16A], $F[11,23] = 7.87$, $p = 0.001$. Tukey's HSD *post hoc* test indicates that values in weeks 10 – 12 are significantly lower than in week 1 at significance level < 0.05). For [$^{125}I_2$]α-CtxArIB[V11L;V16A], $F[11,23] = 19.2$, $p < 0.001$. Tukey's HSD *post hoc* test indicates that values in weeks 3 – 12 are significantly lower than in week 1 at significance level < 0.05). Signal : noise ratio dropped more rapidly for [$^{125}I_2$]α-CtxArIB[V11L;V16A] (time constant = 0.200 wk^{-1}) than for [$^{125}I_1$]α-CtxArIB[V11L;V16A] (time constant = 0.076 wk^{-1}). Lines were generated by non-linear least-squares curve-fitting. r^2 values were 0.793 and 0.975 for the summary fits for [$^{125}I_1$]α-CtxArIB[V11L;V16A] and [$^{125}I_2$]α-CtxArIB[V11L;V16A], respectively. Panel B., Affinity of both ligands remained unchanged over 12 weeks. Although a trend to higher K_d over time was observed for [$^{125}I_2$]α-CtxArIB[V11L;V16A], one-way ANOVA indicated that no significant affinity changes occurred: (for [$^{125}I_1$]α-CtxArIB[V11L;V16A], $F[11,23] = 0.992$, $p = 0.502$, for [$^{125}I_2$]α-CtxArIB[V11L;V16A], $F[11,23] = 1.53$, $p = 0.239$). Lines were generated by non-linear least-squares curve-fitting. r^2 values were 0.504 and 0.357 for the summary fits for [$^{125}I_1$]α-CtxArIB[V11L;V16A] and [$^{125}I_2$]α-CtxArIB[V11L;V16A], respectively. Panel C., Maximum binding values changed over time for [$^{125}I_2$]α-CtxArIB[V11L;V16A] but not [$^{125}I_1$]α-CtxArIB[V11L;V16A]. The B_{max} values measured with [$^{125}I_1$]α-CtxArIB[V11L;V16A] remained constant over 12 weeks (one-way ANOVA shows $F[11,23] = 2.32$, $p = 0.082$),

but fell significantly in the same time period for [$^{125}I_2$]α-CtxArIB[V11L;V16A] (one-way ANOVA shows F [11,23] = 5.55, p = 0.002; Tukey's HSD *post hoc* test indicates that values in weeks 10 – 12 are significantly lower than in week 1 at significance level < 0.05). Lines were generated by non-linear least-squares curve-fitting. r^2 values were 0.089 and 0.057 for the summary fits for [$^{125}I_1$]α-CtxArIB[V11L;V16A] and [$^{125}I_2$]α-CtxArIB[V11L;V16A], respectively.

Figure 6: Inhibition binding at further nAChR subtypes α-CtxArIB[V11L;V16A]

Non-radioactive mono- (hollow points) and diiodinated (filled points) derivatives were generated by cold-iodination at H15 of α-CtxArIB[V11L;V16A]. Inhibition of ligand binding at non-α7 nAChR subtypes was assessed using the same concentrations of α-CtxArIB[V11L;V16A] His-iodinated derivatives as shown in Figure 1. Subtypes probed were: α1β1γδ (2 nM [^{125}I]α-Bgt binding to *Torpedo* electric organ membranes; upward-facing triangles), α4β2* (5 nM [^{3}H]cytisine binding to thalamic membranes; diamonds), α6β2* (0.5 nM [^{125}I]α-CtxMII binding to pooled olfactory tubercle, striatal and superior colliculus membrane; hexagons), α9α10 (5 nM [^{125}I]epibatidine binding to transfected *Xenopus* oocyte membranes; circles), and β4* (0.2 nM [^{125}I]epibatidine + 10 nM A85380 binding to either inferior colliculus, interpeduncular nucleus, or olfactory bulb membranes; the latter is shown here; downward-facing triangles). Points represent mean ± SEM of 3-4 separate determinations. Lines are shown only to connect data points for clarity, no r^2 values were generated for these data as a result.

JPET Fast Forward. Published on March 6, 2008 as DOI: 10.1124/jpet.108.136895
This article has not been copyedited and formatted. The final version may differ from this version.

Figure 1

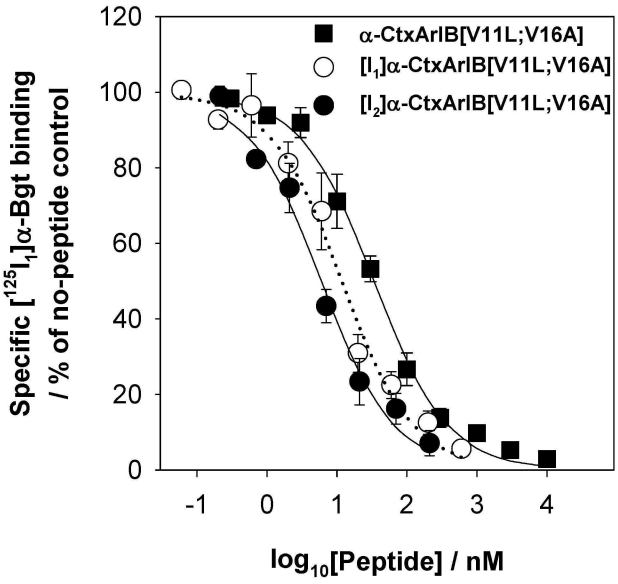

JPET Fast Forward. Published on March 6, 2008 as DOI: 10.1124/jpet.108.136895
This article has not been copyedited and formatted. The final version may differ from this version.

Figure 2

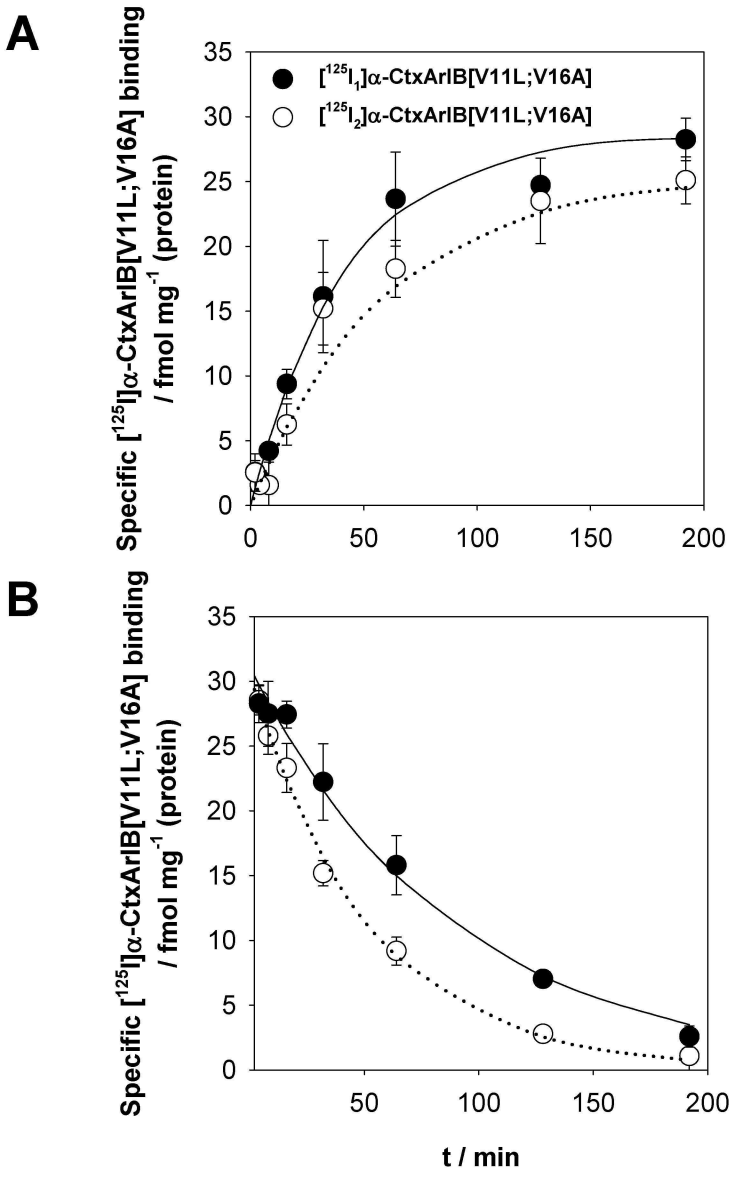

JPET Fast Forward. Published on March 6, 2008 as DOI: 10.1124/jpet.108.136895
This article has not been copyedited and formatted. The final version may differ from this version.

Figure 3

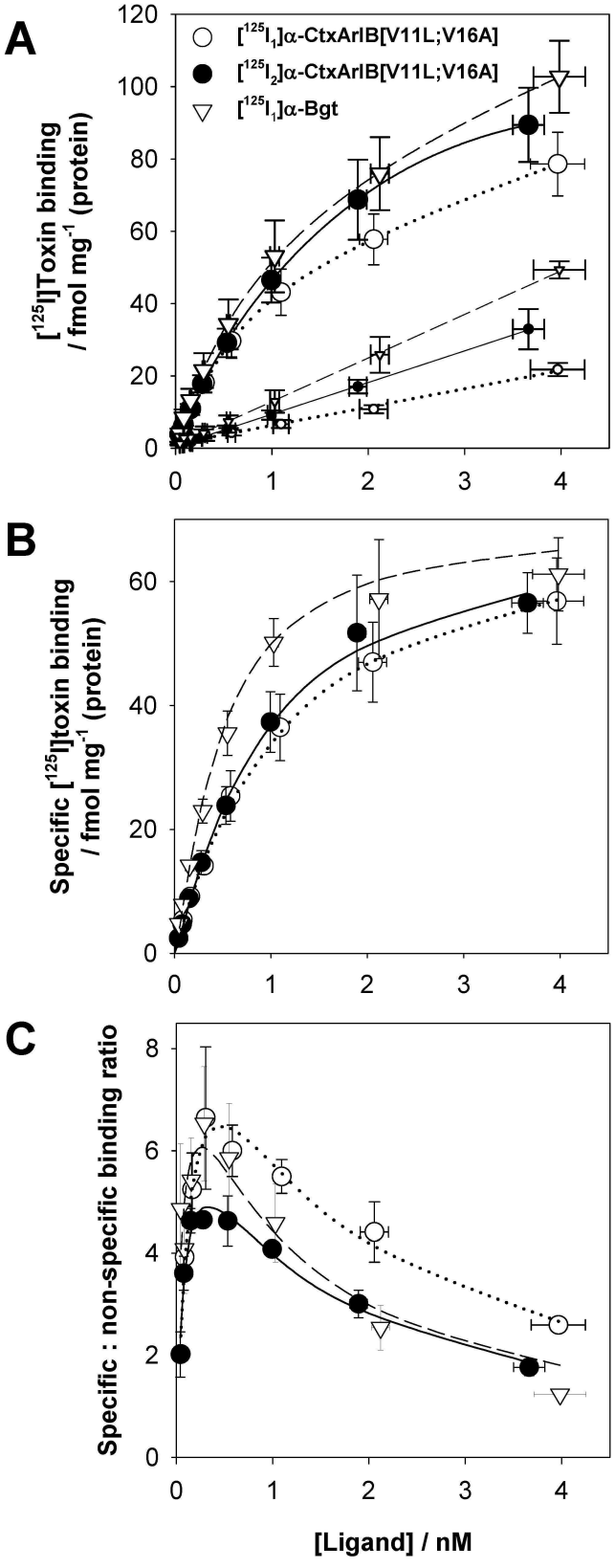

JPET Fast Forward. Published on March 6, 2008 as DOI: 10.1124/jpet.108.136895
This article has not been copyedited and formatted. The final version may differ from this version.

Figure 4

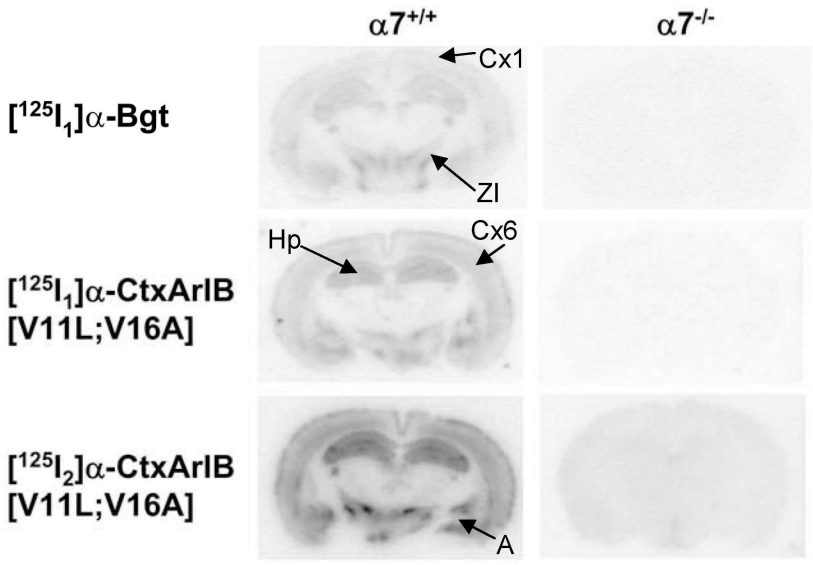

JPET Fast Forward. Published on March 6, 2008 as DOI: 10.1124/jpet.108.136895
This article has not been copyedited and formatted. The final version may differ from this version.

Figure 5

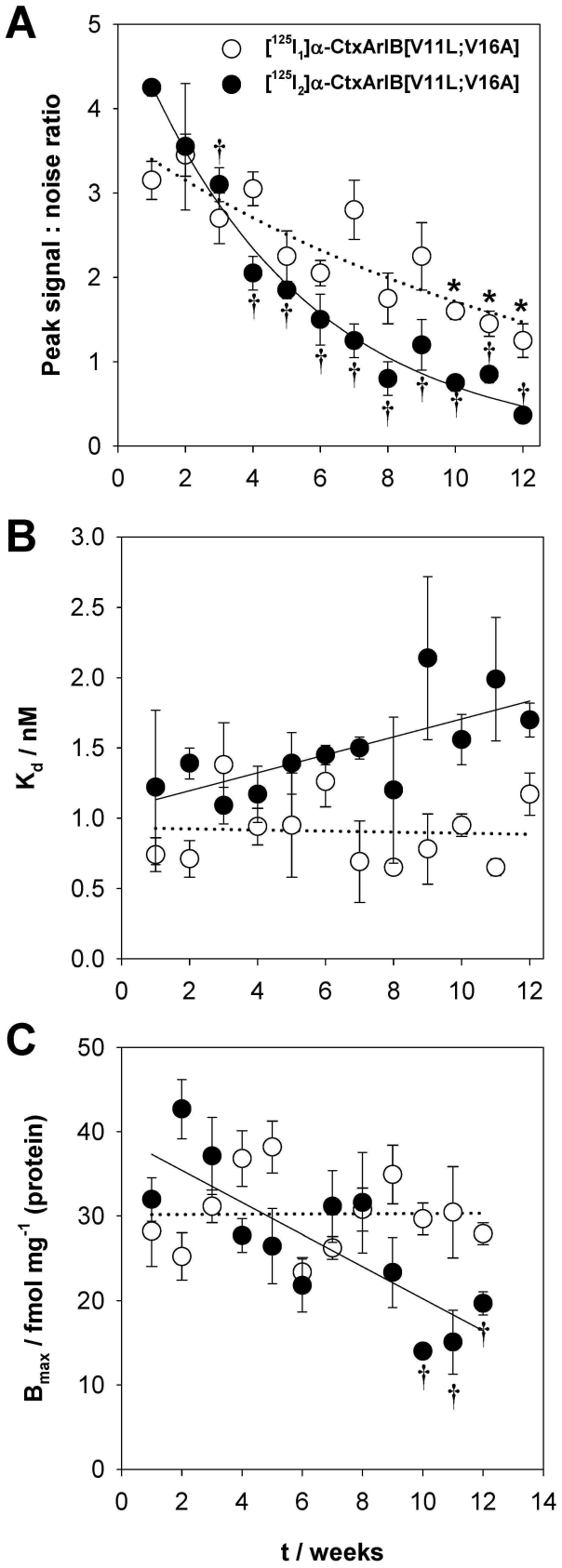

JPET Fast Forward. Published on March 6, 2008 as DOI: 10.1124/jpet.108.136895
This article has not been copyedited and formatted. The final version may differ from this version.

Figure 6